Self-crosslinked polyvinyl alcohol/cellulose nanofibril cryogels loaded with synthesized aminophosphonates as antimicrobial wound dressings

Journal of Materials Chemistry B

ROYAL SOCIETY OF CHEMISTRY

PAPER

View Article Online
View Journal | View Issue

Cite this: J. Mater. Chem. B, 2023, 11, 7144

Self-crosslinked polyvinyl alcohol/cellulose nanofibril cryogels loaded with synthesized aminophosphonates as antimicrobial wound dressings†

Dalia A. Elsherbiny,[ab] Abdelrahman M. Abdelgawad,[*cde] Bahaa A. Hemdan,[f] Ahmed S. Montaser,[c] Ibrahim El-Tantawy El-Sayed,[a] Stefan Jockenhoevel[bg] and Samaneh Ghazanfari*[bg]

Microbial infection is the most common obstacle in the wound healing process, leading to wound healing impairment and complications and ultimately increasing morbidity and mortality. Due to the rising number of pathogens evolving resistance to the existing antibiotics used for wound care, alternative approaches are urgently required. In this study, α-aminophosphonate derivatives as antimicrobial agents were synthesized and incorporated into self-crosslinked tri-component cryogels composed of fully hydrolyzed polyvinyl alcohol (PVA-F), partially hydrolyzed polyvinyl alcohol (PVA-P), and cellulose nanofibrils (CNFs). Initially, the antimicrobial activity of four α-aminophosphonate derivatives against selected skin bacterial species was tested and their minimum inhibitory concentration was determined based on which the most effective compound was loaded into the cryogels. Next, the physical and mechanical properties of cryogels with various blending ratios of PVA-P/PVA-F and fixed amounts of CNFs were assessed, and drug release profiles and biological activities of drug-loaded cryogels were analyzed. Assessment of α-aminophosphonate derivatives showed the highest efficacy of a cinnamaldehyde-based derivative (Cinnam) against both Gram-negative and Gram-positive bacteria compared to other derivatives. The physical and mechanical properties of cryogels showed that PVA-P/PVA-F with a 50/50 blending ratio had the highest swelling ratio (1600%), surface area (523 m^2 g^{-1}), and compression recoverability (72%) compared to that with other blending ratios. Finally, antimicrobial and biofilm development studies showed that the cryogel loaded with a Cinnam amount of 2 mg (relative to polymer weight) showed the most sustained drug release profile over 75 h and had the highest efficacy against Gram-negative and Gram-positive bacteria. In conclusion, self-crosslinked tri-component cryogels loaded with the synthesized α-aminophosphonate derivative, having both antimicrobial and anti-biofilm formation properties, can have a significant impact on the management of uprising wound infection.

Received 24th April 2023,
Accepted 21st June 2023

DOI: 10.1039/d3tb00926b

rsc.li/materials-b

1. Introduction

Wound infection especially bacterial infection could slow down the wound-healing process.[1] The environmental surroundings, such as warm, moist and nutritious wound beds, are perfect conditions for microbial growth;[2] therefore, medicated wound dressings are usually used. Usually, antimicrobial species such as antibiotics and metal nanoparticles are augmented with these dressings to provide sanitation to the wound site.[3,4] Amongst many others, α-aminophosphonate compounds were marked as potent pharmacophores from a drug-design perspective and showed promising biological activity against microbes and exhibited negligible toxicity toward mammalian cells.[5–8]

The dressing materials should have characteristic features such as being biocompatible, biodegradable, easily produced

[a] Department of Chemistry, Faculty of Science, Menoufia University, Egypt
[b] Aachen-Maastricht Institute for Biobased Materials, Faculty of Science and Engineering, Maastricht University, The Netherlands. E-mail: Samaneh.ghazanfari@maastrichtuniversity.nl
[c] Textile Research and Technology Institute, National Research Centre (Affiliation ID: 60014618), Dokki, Cairo, Egypt. E-mail: aabdelg@ncsu.edu
[d] Textile Engineering Chemistry and Science Department, Wilson College of Textiles, North Carolina State University, Raleigh, NC, USA
[e] Chemistry Department, Faculty of Science, New Mansoura University, New Mansoura City 35511, Egypt
[f] Water Pollution Research Department, National Research Centre, 33 El-Bohouth St., Dokki, Giza 12622, Egypt
[g] Department of Biohybrid & Medical Textiles (BioTex), AME-Helmholtz Institute for Biomedical Engineering, RWTH Aachen University, Forckenbeckstrabe 55, 52072 Aachen, Germany

† Electronic supplementary information (ESI) available. See DOI: https://doi.org/10.1039/d3tb00926b

and able to successfully restore their activity until reaching the target sites. Moreover, they should maintain a moist environment around the wound to enhance healing,[9] enable continuous wound site monitoring, allow the exchange of gases, and prevent subsequent infection of the wound and they should have a wide range spectrum of antimicrobial activity.[10] Choosing appropriate dressing is a significant decision in wound management.

Numerous carriers such as hydrogels,[11,12] foam, porous aerogels, cryogels,[13–15] films and others have been used in the wound care sector.[16–18] Cryogels and their analogues xerogels and aerogels are classes of lightweight porous materials that are obtained by replacing the solvent in the gel with air without any significant change in the material network structure or the volume of the gel itself.[19] Besides the high surface area, high porous structure and low densities, these gels possess other noteworthy properties such as low thermal conductivity, high strength (in most cases), low dielectric permittivity and extraordinary water uptake properties.[20] The uniqueness of porous wound healing materials appears in the case of chronic wounds, where exudates and pus need to be removed frequently. Moreover, high drug loads can be offered through the pores to provide burst release to infected wounds.[21] Cryogels can be obtained using the freeze–drying technique and most hydrophobic molecules and water-insoluble drugs can be incorporated *via* dispersion in the base polymer solution.[22] Cryogels from biopolymers such as polyvinyl alcohol (PVA), chitosan, curdlan, carrageenan, and carboxymethyl cellulose have been reported as excellent medicated wound dressings.[23–25]

PVA is a sustainable base material and it is among the few vinyl polymers that dissolve in water, contributing to its biodegradability. Additionally, PVA possesses other promising features such as biocompatibility, nontoxicity, chemical resistance, and elasticity. Its functions are based on its molecular weight and degree of hydrolysis, which impacts the number of attached hydroxyl groups.[26] Due to its plentiful hydroxyl groups, PVA also has gas barrier qualities, is easy to produce films, and demonstrates beneficial bonding interactions so that it has been used significantly for pharmaceutical purposes. PVA cryogels are specifically suitable for wound healing applications because of their porous and hydrophilic nature, which allows them to absorb large volumes of exudate; nevertheless, they lack mechanical strength and integrity.[27,28] Therefore; their performance has been improved through post-treatment, chemical cross-linking *via* glutaraldehyde, glyoxal and epichlorohydrin,[29] and the introduction of reinforcing agents including cellulose fillers, such as nanofibrils (CNFs) and nanocrystals (CNCs). It is worth mentioning that chemical crosslinkers are quite toxic to humans.

The hydroxyl groups in a cellulose structure can form strong fibril networks through inter- and/or intra-chain hydrogen bonding which in turn endows the material with high mechanical strength.[30] It is worth mentioning that fully hydrolyzed PVA exhibits self-crosslinking properties upon cooling due to high chain packing.[31] Nanocellulose is also ideal for a wound dressing material because of its high ability to absorb exudates and its outstanding compaction properties.[32–34] However, a crosslinker with some degree of cytotoxicity such as glutaraldehyde and epichlorohydrin[35] has to be introduced to the PVA/CNF system to control its water solubility. Therefore, there is a need for the development of benign but effective wound dressing systems.

In this study, we carried out the fabrication of a potent antimicrobial wound dressing cryogel from a PVA/CNF system. The antimicrobial properties were acquired through the preparation of four new drugs based on α-aminophosphonate by reacting 4-(4-chlorophenyl)thiazol-2-amine and four different aldehydes, namely, syringaldehyde, anisaldehyde, phenylacetaldehyde, and cinnamaldehyde. Triphenylphosphite was utilized as a precursor of phosphorus nuclei while glacial acetic acid served as both a catalyst and a solvent. To our knowledge, there are no previous studies on such self-crosslinked tri-component systems in the literature. We propose that incorporating fully hydrolyzed PVA into a cryogel system would induce self-crosslinking properties hence avoiding the cytotoxic effects of chemical crosslinkers, enhancing the mechanical strength, preventing disintegration upon wetting, and imparting sustained release behavior to the system. The chemical assemblies of the synthesized products were proven by the following characterization studies: Fourier transform infrared (FT-IR), Nuclear Magnetic Resonance (^{1}H-NMR, ^{13}C-NMR, and ^{31}P-NMR) and Mass Spectrometry (MS). The biological activity of the synthesized compounds was screened against some selected skin bacterial pathogens that are widely related to hospital-acquired infections, namely *Acinetobacter baumannii* and *Pseudomonas aeruginosa* in Gram-negative species and *Staphylococcus aureus* and *Streptococcus mutans* in Gram-positive species. The minimum inhibitory concentration of the synthesized molecules was determined, and the most efficient one was loaded into a PVA-based cryogel system for developing an antimicrobial delivery system for wound care purposes. The cryogel structure is a self-crosslinked tri-component system from fully hydrolyzed PVA, partially hydrolyzed PVA, and CNFs. Finally, the antibacterial activity of the loaded cryogel and its antibiofilm performance were evaluated.

2. Materials and methods

2.1. Materials

Solvents and chemicals such as 4-(4-chlorophenyl)thiazol-2-amine, syringaldehyde, anisaldehyde, phenylacetaldehyde, cinnamaldehyde, triphenylphosphite, and acetic acid required for the synthesis of α-amino phosphonates, polyvinyl alcohol (87–90% Met. 30 000–70 000), and polyvinyl alcohol (99%, Mwt. 30 000) were obtained from Sigma-Aldrich, USA, and used without further purification. Deionized water was used to prepare solutions and suspensions. Cellulose nanofibrils were kindly provided as a 3% slurry from Sappi Global (Maastricht, the Netherlands).

2.2. Synthesis of α-aminophosphonate derivatives

Equimolar concentrations of 4-(4-chlorophenyl)thiazol-2-amine, different aldehydes 1–4 (Scheme 1), and triphenylphosphite were added to 5 mL of glacial acetic acid and stirred at 80 °C for eight hours. Thin layer chromatography (TLC) was employed

to track the progress of the reaction until all of the starting materials had been consumed. Glacial acetic acid was evaporated once the reaction was complete, and the sticky residue was then treated with diethyl ether to produce solid particles. To obtain pure α-aminophosphonate compounds in a good yield, the precipitate from methylene chloride/ethyl acetate (1 : 2) was filtered out and crystallized.[36]

The products were coded according to the parent aldehydes syringaldehyde, anisaldehyde, phenylacetaldehyde, and cinnamaldehyde as Syring, Anis, Phenylact, and Cinnam, respectively.

2.3. Fabrication of the polyvinyl alcohol/cellulose nanofibril cryogel and drug loading

Solutions of partially hydrolyzed PVA (PVA-P) and fully hydrolyzed PVA (PVA-F) were dissolved in distilled water at 2 w/v% and kept under stirring for 6 h at 60 °C. A suspension of CNFs (1.5 wt%) was prepared and kept in a fridge for further use. A series of PVA-P and PVA-F blends (CG-1, CG-2, CG-3, and CG-4) were prepared by mixing desired volumes of each polymer according to Table 1. Solutions for cryogels were prepared by mixing PVA-P and PVA-F blends with a fixed amount of CNF suspension (10 mL) to bring the final volume to 20 mL for each sample. These solutions were kept stirred for 12 h at room temperature to ensure better homogeneity, then, poured into plastic containers of 5 mL volume and placed in a freezer overnight. The samples were moved from the freezer to the freeze-drying unit and kept for 24 h until complete drying was achieved.

The samples were removed from the plastic containers gently and their morphology, swelling and mechanical compression

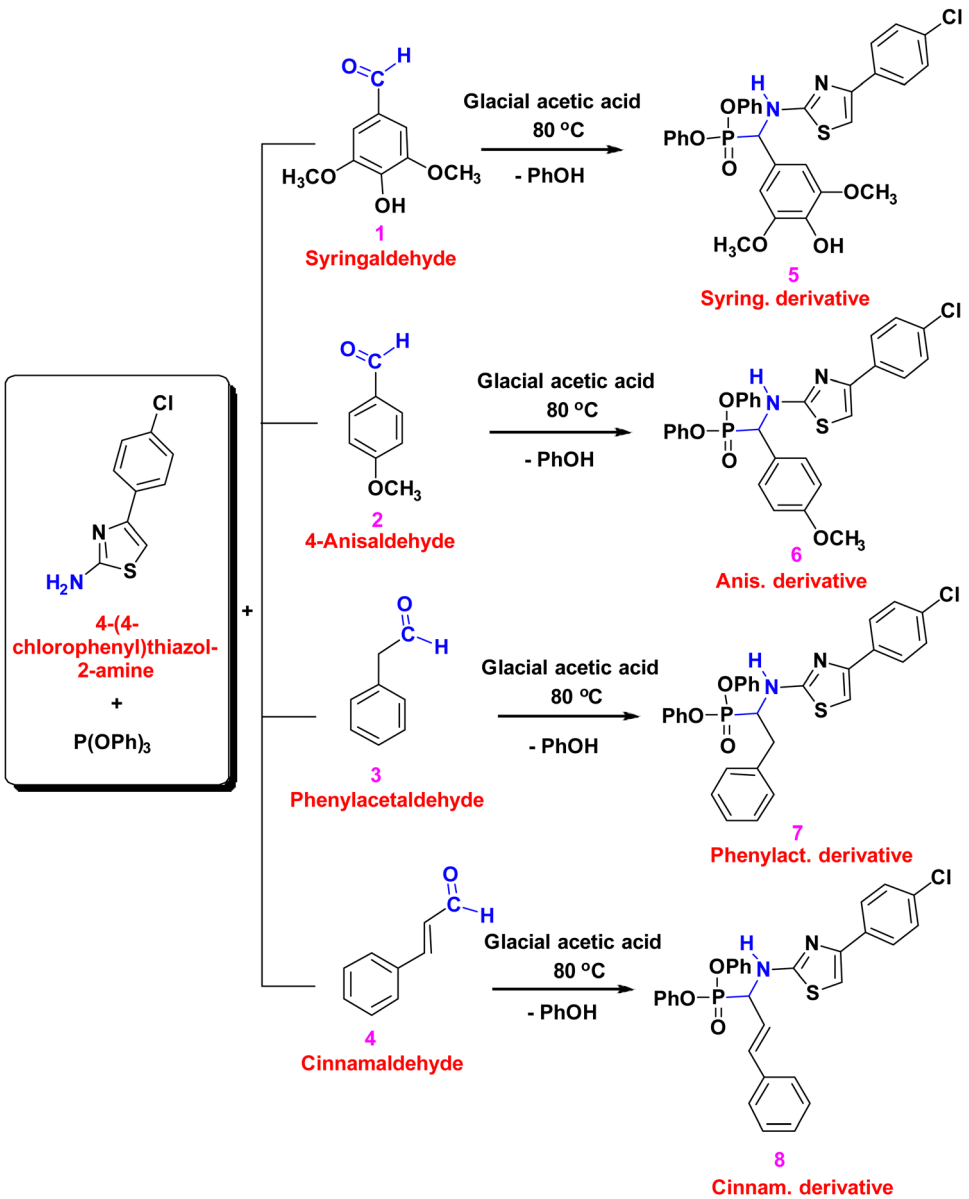

Scheme 1 Synthesis of α-aminophosphonates from 4-(4-chlorophenyl)thiazol-2-amine, different amines and triphenylphosphite.

Table 1 Cryogel blending ratios

Code	PVA-P to PVA-F blending ratio	PVA-P (mL)	PVA-F (mL)	CNFs (mL)
CG-1	95/5	9.5	0.5	10
CG-2	90/10	9	1	10
CG-3	80/20	8	2	10
CG-4	50/50	5	5	10

properties were investigated. The optimum cryogel sample with superlative water stability and mechanical properties was identified and used to determine the most effective antimicrobial drug by loading four different aminophosphonate concentrations of 0.25, 0.5, 1, and 2 mg/5 mL into the polymer blend coded as CG4-1, CG4-2, CG4-3, and CG4-4, respectively. Before the formulation of the cryogel, the antimicrobial aminophosphonate precursor was added to the polymer mixed solutions.

2.4. Chemical identification of the synthesized α-aminophosphonate compounds

DMSO-d6 was used as the solvent for the ^{1}H-NMR, ^{13}C-NMR, and ^{31}P-NMR tests, which were performed using 500 MHz Varian, 500 MHz Varian, and Bruker Avance (the USA) spectrometers. FTIR spectroscopy testing was performed using a Thermo Nicolet (USA). Chemical changes related to the specific solvent were recorded in ppm. Chemical shifts (δ) were measured relative to the appropriate solvent as an internal reference and recorded in parts per million (ppm). Standard abbreviations were recorded (b → broad; s → singlet; d → doublet; m → multiplet). Using a Shimadzu QL 800 15–70 V, mass spectroscopy tests were confirmed to ascertain the purities of the identified compounds. TLC on Kiesel gel (F254, Merck) precoated plates was used to control and monitor the progress of the reaction. The reaction mechanism is presented in Scheme 2 and the collected data are summarized as follows:

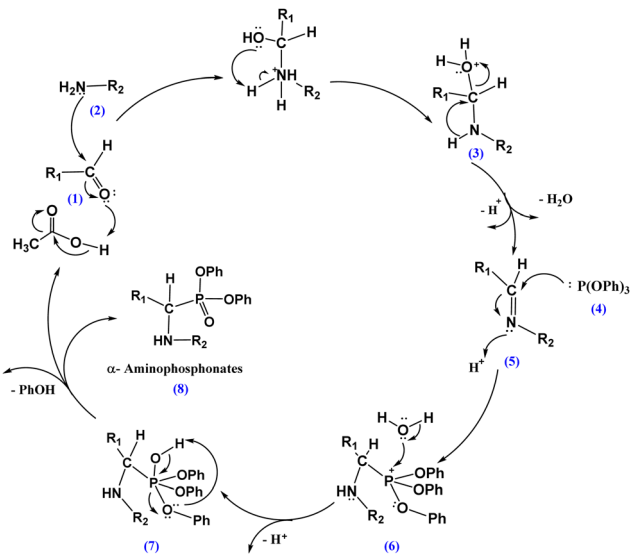

Scheme 2 Proposed mechanism for aminophosphonate derivatives.

Compound 5: diphenyl-((4-(4-chlorophenyl)thiazol-2-yl)amino)-(((4-hydroxy-3,5-dimethoxyphenyl)methyl)phosphonate. Purple color, yield (93%), FTIR, (cm^{-1}): 3239–3400 (br., NH, OH), 1593 (C═C, Ar.), 1192 (P═O), 759 (P–C). ^{1}H-NMR (500 MHz, DMSO, ppm) δ = 8.06–6.25 (m, 17H), 5.68 (s, 1H, NH), 5.07 (d, J = 26.8, 1H, NCHP), 3.74 (s, 6H, 2OCH$_3$). ^{13}C-NMR (75 MHz, DMSO) δ = 159.27, 150.30, 150.21, 147.39, 130.80, 130.53, 130.22, 129.76, 129.05, 125.75, 120.59, 114.88, 114.00, 113.80, 65.38, 55.62. ^{31}P-NMR (500 MHz, DMSO, ppm) δ: 15.51. LCMS, m/z ($C_{30}H_{26}ClN_2O_6PS$) calcd, 609.03; found, 609.05 [M]$^+$.

Compound 6: diphenyl-((4-(4-chlorophenyl)thiazol-2-yl)amino)-(((4-methoxyphenyl)methyl)phosphonate. Pink color, yield: 95%, FTIR (cm^{-1}): 3180–3321 (br., NH, OH), 1589 (C═C, Ar.), 1249 (P═O), 829 (C–Cl), 759 (P–C). ^{1}H NMR (500 MHz, DMSO, ppm) δ = 8.38–6.15 (m, 19H), 5.68 (s, 1H, NH), 5.01 (d, J = 26.8, 1H, NCHP), 3.69 (s, 3H, OCH$_3$). ^{13}C NMR (75 MHz, DMSO) δ = 157.87, 150.44, 148.01, 147.60, 130.26, 129.95, 129.92, 129.60, 121.07, 121.01, 120.81, 119.35, 115.79, 115.32, 65.47, 56.12. ^{31}P-NMR (500 MHz, DMSO, ppm) δ: 15.74; LCMS, m/z ($C_{29}H_{24}ClN_2O_4PS$) calcd, 563.00; found, 563.09 [M]$^+$.

Compound 7: diphenyl-(1-((4-(4-chlorophenyl)thiazol-2-yl)-amino)-2-phenylethyl)phosphonate. Light brown color, yield (94%), FTIR (KBr) cm^{-1}: 3198–3390 (br., NH, OH), 1593 (C═C, Ar), 1203 (P═O), 752 (P–C), 690 (C–Br). ^{1}H NMR (500 MHz, DMSO, ppm) δ = 8.27–6.20 (m, 20H), 5.72 (s, 1H, NH), 5.07 (d, J = 4.8, 1H, NCHP), 2.21–1.45 (m, 2H). ^{13}C NMR (500 MHz, DMSO) δ = 165.19, 157.79, 155.97, 155.36, 138.13, 137.78, 137.60, 137.23, 136.63, 136.48, 133.82, 127.89, 127.83, 126.67, 123.10, 64.00, 30.30. ^{31}P-NMR (500 MHz, DMSO, ppm) δ: 15.81; LCMS, m/z ($C_{29}H_{24}ClN_2O_3PS$) calcd, 547.01; found, 547.99 [M + 1]$^+$.

Compound 8: diphenyl-(*E*)-(1-((4-(4-chlorophenyl)thiazol-2-yl)-amino)-3-phenylallyl)phosphonate. Yellow color, yield (95%), FTIR (KBr) cm^{-1}: 3155–3310 (br., NH, OH), 1589 (C═C, Ar.), 1184 (P═O), 756 (P–C). ^{1}H NMR (500 MHz, DMSO, ppm) δ = 8.04–6.94 (m, 20H), 6.91–6.57 (m, 2H, HC═CH), 5.69 (s, 1H, NH), 4.25 (dd, J = 24.5, 8.2, 1H, NCHP). ^{13}C NMR (500 MHz, DMSO) δ = 161.95, 153.56, 151.66, 149.65, 139.37, 137.34, 137.07, 136.91, 136.24, 135.58, 131.06, 130.26, 126.63, 125.92, 121.37, 119.31, 117.72, 61.59. ^{31}P-NMR (500 MHz, DMSO, ppm) δ: 21.65; LCMS, m/z ($C_{30}H_{24}ClN_2O_3PS$) calcd, 559.02; found, 559.50 [M]$^+$.

2.5. Screening the biological activity of the synthesized α-aminophosphonate compounds

2.5.1. Microorganisms used and conditions. The bactericidal features of the four synthesized drugs were appraised against some selected skin bacterial pathogens obtained from American Type Culture Collection Center (ATCC, USA). The most widely and clinically relevant species of bacteria in hospital-acquired infections, namely *Acinetobacter baumannii* and *Pseudomonas aeruginosa* in Gram-negative species and *Staphylococcus aureus* and *Streptococcus mutans* in Gram-positive species, were selected for the corresponding antibacterial susceptibility test.

The lyophilized inoculum of bacterial stocks was reactivated, according to El Nahrawy *et al.*[34] by placing 100 μL into a tube containing trypticase soy broth (TSB). Afterward, the inoculation

tubes were aerobically kept at 37 °C in an incubator for 18–24 hours to make fresh bacterial suspensions, which were centrifuged for 10 min at 5000 × *g* rpm. The pellets, which contained pure cells, were re-suspended with PBS. The absorbance of the cultured broth medium was measured spectrophotometrically at 600 nm and adjusted to 0.5 McFarland's turbidity standard to accomplish 1.5×10^8 CFU mL^{-1}. Before undertaking antibacterial experiments, the standard solution of all synthesized drugs (100 mg mL^{-1}) was sonicated for 15 min. All experiments were carried out in three repetitions over three days.

2.5.2. Antibacterial activity tests using agar diffusion assay. The antibacterial performance of the four synthesized drugs (Syring, Anis, Phenylact, and Cinnam) was investigated using a zone of inhibition assay against the selected pathogenic species, including *A. baumannii*, *P. aeruginosa*, *S. aureus*, and *Str. mutans*. The disc diffusion method was conducted under aseptic conditions. A 0.1 mL of individual bacterial suspension was disseminated thoroughly on a Mueller–Hinton agar (MHAm Sigma-Aldrich, UK) plate with a sterile cotton swab. The used filter paper discs (6 mm in diameter), which were impregnated with 50 μL of all synthesized drugs, were positioned on the surface of the seeded MHA plates with the bacterial inoculum.

Concerning the well-diffusion assay, the uniform wells (6 mm) were drilled in the deep layer of the seeded MHA agar. In the next phase, each well was injected with 50 μL of the stock solution.[37] Ciprofloxacin (30 μg mL^{-1}) was applied as reference antibiotics against individual bacterial species. All Petri dishes were placed upside down in an incubator at 37 °C for 18–24 h, and the width of the zone of inhibition (ZOI) formed around the discs and wells was measured using a ruler. The experimentation was done in triplicate, and values of ZOI were presented as mean ± SD.

2.5.3. Evaluation of the minimum inhibitory concentration (MIC) and the minimum biocidal concentration (MBC). Using the broth microdilution technique, the MIC and MBC values of four synthesized drugs against selected pathogenic bacterial strains were estimated according to El Nahrawy *et al.* 2021c. Each drug was diluted with PBS to the final three various dosages (50, 100, 150, and 200 μg mL^{-1}) and then transferred into a sterile test tube with 5 mL of distilled water. The tubes were further supplemented with 100 μL (107 CFU) of log-phase bacterial suspension that was prepared previously. A tube injected with a bacterial suspension without adding the synthesized drugs was employed as a negative control. Afterward, the experimental inoculated and control tubes were placed in a shaker with an agitation speed of 200 rpm. The inhibition of bacterial growth was determined by withdrawing 0.1 mL of each tube at varying exposure times (30, 60 and 90 min). The heterotrophic plate counts (HPCs) of bacterial populations were determined using plate count cell viability methods.[38]

2.6. Physical, mechanical, and biological characterization of PVA-P/PVA-F/CNF cryogels

2.6.1. Surface morphology using FESEM. A Field Emission Scanning Electron Microscope (FESEM), FEI Verios 460L, USA, was used to explore the cryogel morphology. A sharp, clean blade was used to fracture the cryogels under liquid N_2; afterward these cryogels were imaged in the radial cross-section. Double-sided carbon tape was used to attach the samples to the metal stub. A layer of gold and platinum measuring 5 nm thick was applied to the SEM samples after they had been produced.

2.6.2. Surface area using BET method. The surface area of the created cryogels was evaluated using Brunauer–Emmett–Teller (BET) analysis with a Nova LX. Volumetric adsorption equipment (BELSORP-mini II, Nippon Bell, Osaka, Japan) operating at the liquid nitrogen temperature was used to measure the amount of nitrogen that adsorbed to the catalysts. The *t*-plot method was employed to identify the inner and outer surface areas. Using the Barrett–Joyner–Hallender (BJH) model, the pore size distribution curve has been calculated from an adsorption branch.

2.6.3. Swelling and structure integrity. In order to achieve equilibrium swelling, each dried cryogel sample was swollen in deionized water for 24 hours at room temperature. Periodically, samples were taken out, blotted dry using tissue paper, and weighed. In accordance with eqn (1), the swelling ratio was computed. In order to obtain accurate results, each analysis was carried out three times

$$\text{Swelling ratio} = \frac{\text{Wet weight} - \text{Dry weight} \times 100\%}{\text{Dry weight}} \quad (1)$$

2.6.4. Mechanical compression tests. In a flat-bottomed, cylindrical plastic container, the formulated cryogels were molded for compression testing. Cylindrical cryogels were sliced with a clean, sharp blade to remove the top and bottom overhangs. Compression recoverability (RC) was obtained with a Kawabata Evaluation System (KES-FB3-A, Japan). The compression area was 2 cm^2 and the maximum load was 50 gf cm^{-2} with a speed of 0.002 cm s^{-1}. Values closer to 100 mean better recoverability and higher compression resistance.

2.6.5. Drug release properties. Triplicates of the *in vitro* drug release tests for the Cinnam derivative from CG-4 cryogels were carried out. Precisely, 100 mL of phosphate buffered saline (pH 5.5) was added to a beaker containing 100 mg of dry cryogel, and the beaker was shaken (50 cycles per minute) at 37 °C in a shaking bath. At predetermined intervals (between 30 min and 75 h), the samples were removed and fresh phosphate buffer was added in their stead. The amount of the aminophosphonate compound that had been released was measured by determining UV absorbance at a wavelength of 277 nm in a single beam spectrophotometer (Shimatzu – UV1601 PC, England).[39]

2.7. Biological activity of α-aminophosphonates loaded cryogels

2.7.1. *In-vitro* antibacterial activity of cryogels. The antibacterial properties of the studied cryogels as promising wound dressings were assessed *in vitro* against selected pathogenic bacteria namely *A. baumannii*, *P. aeruginosa*, *S. aureus*, and *Str. mutans* using the agar diffusion assay. The swatches with a particular size (5 × 5 cm^2) of each cryogel were placed onto the top layer of the MHA plate in the disc diffusion assay.

2.7.2. Bacterial growth inhibition tests of the studied cryogels. Bacterial cells were injected into new media with a designated species of individual cryogels (5×5 cm^2) for proliferation inhibitory testing. The cryogel of the desired size was immediately implanted in a sterile collection tube with 10 mL of DW for Gram-negative and Gram-positive bacteria. The tubes were then injected with a 10 μL of fresh bacterial suspension and maintained in a shaking incubator at 37 °C with an agitation speed of 200 rpm for a particular span of contact time (2 to 10 h). A portion of the mixture was fetched from each group during co-incubation with cryogels. By plating successive dilutions on TSA media incubated at 37 °C for 24 h, the bacteria cell density (CFU mL^{-1}) was quantified.[40] The following equation was utilized to estimate the bacterial log CFU reduction:

$$\text{Log CFU reduction} = \text{Log CFU control} - \text{Log CFU after exposure to cryogels}$$

2.7.3. Reduction of biofilm colonization. Microbial colonization of wounds experiments was conducted to prohibit biofilm production over wounds. For assessing the monospecific biofilm formation of each selected pathogen, a cryogel swatch of a particular size was immersed into tubes containing 10 mL of PBS, and then each tube was injected with 50 μL of 24 h fresh bacterial suspensions. All injected tubes were marinated at 35 °C and 80% relative humidity at a constant position to allow bacterial adhesion over the cryogel. Following that, at 0 day of incubation, the bacterial adhesion and biofilm formation over each swatch was scraped according to Hemdan *et al.*[41] After each interval, the cell viability of detached biofilm was performed and used to calculate the mean colony forming units (CFU cm^{-2}).

2.7.4. Biocompatibility and toxicity assays. The toxicological profiles of four cryogels were evaluated using a Microtox® Model 500 (M500) analyzer (Modern Water Inc., New Castle, DE, USA), which is considered the common technique used to evaluate toxicity to ensure their efficacy and suitability in biological applications.[42]

3. Results and discussion

3.1. Chemistry of the synthesized α-aminophosphonate compunds

Several synthesis methods were recorded in the literature for the synthesis of α-aminophosphonates.[36,43] In the current study, novel α-aminophosphonate-based drugs with expected biological activity were prepared using acetic acid as a solvent and catalyst at 80 °C.[44] Four different aldehydes were utilized in the synthesis process, along with the following amine; 4-(4-chlorophenyl)thiazol-2-amine (Scheme 1). Some techniques (IR, ^{1}H-NMR, ^{13}C-NMR, ^{31}P-NMR and Mass spectrometry) were used to interpret and investigate the chemical structures of the prepared α-aminophosphonate molecules (5–8).

The proposed mechanism of the synthesis of α-aminophosphonate based compounds by glacial acetic acid as a catalyst and solvent is presented in Scheme 2. The mechanism of the reaction is believed to be following the path of activation of aldehyde as well as the *in situ* generated imine (Schiff base) by protonation of the nucleophilic carbonyl oxygen of the aldehyde (**1**) by acetic acid in the first step. This facilitates the nucleophilic addition of the amino group nitrogen of the heterocyclic amine component (**2**) to the electrophilic carbon followed by dehydration as in compound (**3**). The nucleophilic addition of the triphenyl phosphite phosphorus (**4**) to the electrophilic carbon of the >C═N bond of the imine (**5**) led to the *in situ* generation of phosphonium salt (**6**) as an intermediate. In the final step, the addition of water to this phosphonium salt liberating the end product (**8**) through the formation of the hydroxyphosphite intermediate (**7**) followed by the elimination of phenol as shown in Scheme 2.

The FT-IR spectra of all the synthesized α-aminophosphonate compounds presented in the ESI† (S1–S4) show a broad peak at 3155–3400 cm^{-1} which corresponds to the –NH and –OH groups. Also, the stretching band of CH–aromatic is observed at 1589–1593 cm^{-1}. A band is noticed at 1184–1249 cm^{-1} corresponding to P═O, and P–C is absorbed at 752–759 cm^{-1}.

The ^{1}H-NMR spectra of all derivatives in DMSO are presented in the ESI† (S5–S8). The ^{1}H-NMR spectra of compounds **5**, **6**, **7** and **8** show singlet peaks at δ values (ppm) of 5.68, 5.68, 5.72 and 5.69, respectively, belonging to (NH). Additionally, doublet peaks are noticed at δ values (ppm) of 5.07, 5.01, 5.07 and 4.25, respectively, corresponding to (NCHP). On the other hand, singlet peaks at δ values (ppm) of 3.74 and 3.69 are attributed to the (methoxy groups) of compounds **5** and **6**, respectively.

^{13}C-NMR spectra for compounds **5**, **6**, **7** and **8** (S5–S8) show signals at δ values (ppm) of 159.27, 157.87, 165.19, and 161.95, respectively, which correspond to the C═N, thiazole ring, while signals observed at δ values (ppm) of 150.30, 150.44, 157.79 and 153.56, respectively, are attributed to (P–O–Ph). However, in compound **5**, the signal at 150.21 corresponds to (C–OH, Ar.). Additionally, signals that appeared at δ values (ppm) of 147.39, 148.01, 155.97 and 151.66, respectively, belong to the C–S, thiazole ring. On the other hand, the peaks at δ values (ppm) of 65.38, 65.47, 64.00 and 61.59, respectively, correspond to the C–H, chiral. However, signals at δ values (ppm) of 55.62 and 56.12 are attributed to the methoxy groups of compounds **5** and **6**, respectively. Finally, the signal that appeared at a δ value (ppm) of 30.30 corresponds to the CH_2 of compound **7**. The ^{31}P-NMR spectra of compounds **5**, **6**, **7** and **8** show single peaks at δ (ppm) 15.74, 15.51, 20.19 and 21.82, respectively.

3.2. Biological activity of the synthesized α-aminophosphonate compounds

3.2.1. Qualitative screening using the disk diffusion method. The present investigation reported the size of the ZOI for four studied synthesized drugs (Syring, Anis, Phenylact, and Cinnam) against four selected pathogenic bacteria namely *A. baumannii*, *P. aeruginosa*, *S. aureus*, and *Str.mutans*, as represented graphically in Fig. 1. The qualitative antibacterial screening test displayed a potent growth inhibitory impact of the Cinamm against all selected pathogens with a large ZOI, where their average ZOI

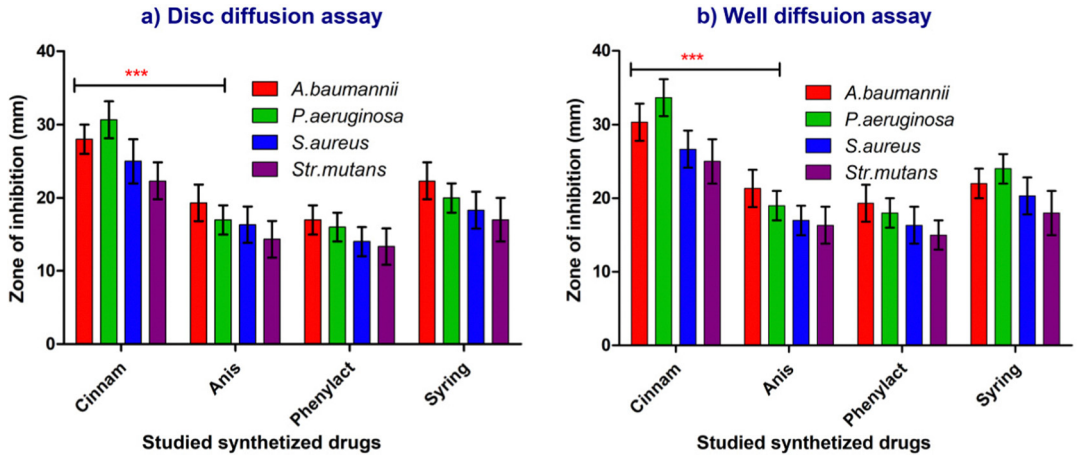

Fig. 1 Antibacterial behavior of four explored synthesized drugs against four skin bacterial pathogens using (a) the agar diffusion assay, and (b) well diffusion assay. The ZOI width (mean ± SD) is represented in mm. *** with $P > 0.0001$ indicated a strong significance between all tested materials and bacterial strains.

diameters against *A. baumannii*, *P. aeruginosa*, *S.aureus*, and *Str.mutans* were recorded as 28, 30.66, 25 and 22.3 mm, respectively, using the disc diffusion assay, and 30.3, 33.7, 26,6, and 25 mm, respectively, using the well diffusion assay. With respect to the antibacterial action of ciprofloxacin, the results indicated that the widths of the ZOI obtained using the disc assay were 25, 22, 19 and 17 mm for. *baumannii*, *P. aeruginosa*, *S. aureus*, and *Str.mutans*, respectively.

On the other hand, the weak inhibitory impact against selected pathogenic bacteria was recorded to Anis and Phenylact, and the limited ZOI was determined compared with Syring which is considered the most potent antibacterial compound. The results revealed that the width of the ZOI obtained by the well diffusion assay was larger than that obtained by the disc diffusion assay. This may be due to the high diffusion of bioactive ingredients that could explain this phenomenon in the agar media. This argument is consistent with the findings of El Nahrawy *et al.*[40] where similar observations were found. The significance of this result can be most meaningful because it can help select the best drugs with a strong antibacterial effect. Hence, further experimental works were conducted to evaluate these drugs' biocidal effects using quantitative techniques, including the determination of MICs.

3.2.2. Determination of the antimicrobial efficacy of Cinnam drug *via* the colony forming unit (CFU) method. The broth dilution assay was used to determine the effective dosage and time of drugs required to completely eliminate the bacterial populations of *A. baumannii*, *P. aeruginosa*, *S. aureus*, and *Str. mutans*. The experimental results of the *in vitro* antibacterial profile of the tested drugs mentioned above showed that Cinnam displayed higher antibacterial efficiency than other drugs. They fully prohibit bacterial growth (log 6 CFU mL^{-1}) at low dosages and the lowest treatment time (30 min) was recorded. As shown in Fig. 2, the MIC values were observed to be 150 μg mL^{-1} at 60 min for *P. aeruginosa*, 150 μg mL^{-1} at 90 min for *A. baumannii*, and 200 μg mL^{-1} at 60 min for *S.aureus* and *Str.mutans*. Synthesized drugs Anis and Phenylact could not completely hinder the growth of *Str.mutans* up to a dosage of 200 μg mL^{-1} within 90 min (Fig. 3 and 4). These results are in line with the results reported by He *et al.*,[42] in which the bactericidal action of Cinnam against *E. coli*, *S. aureus*, and *Enterococcus faecalis was assessed*. This phenomenon can be adequately explained by the reality that Cinnam could damage bacterial DNA. *SulA* transcription is a stress marker, as it elevates after DNA damage, and it might be used as a preliminary step for an investigation into the mechanism of action of antibacterial options [ref].

Furthermore, using membrane and gene regulation, Cinnam's antibacterial strategy towards Gram-negative *E.coli* was also addressed. Malheiro *et al.*[45] investigated Cinnam on three important pathogens, *E. coli*, *S. aureus*, and *Enterococcus*, comparing their findings to those of the antibacterial compound; the researchers discovered that Cinnam suppressed *E. coli* at the small dosage and diminished growth of microorganisms similar to the result of this study. In turn, Yuan *et al.*[46] utilized the Time-Kill approach to assessing the potential interruption of bioactive substances on bacterial evolution, and it was uncovered that Cinnam had excellent antimicrobial properties, specifically in combination with eugenol, another component of Cinnam essential oil. The destruction they exacerbated to the cell wall was considered to be the significant cause. As a consequence, the outcomes displayed that Cinnam was efficacious in treating pathogenic bacteria and established as a desirable candidate compound for antibacterial discovery.[47]

A moderate inhibitory effect against selected pathogens was found for the Syring compound, where 200 μg mL^{-1} min was the MIC value for *A. baumannii* and *P. aeruginosa*, within 60 min and *S. aureus* and *Str.mutans* within 90 min (Fig. 5). A notable feature of this study is that from the antibacterial profile, it could be summarized that the Syring drug exhibited a broad spectrum of bactericidal effects, being vigorous against both Gram-positive and Gram-negative bacterial strains. This highlights the potential of Cinnam to be loaded in the cryogels to improve the antibacterial profile and prohibit biofilm production. Syring is a naturally

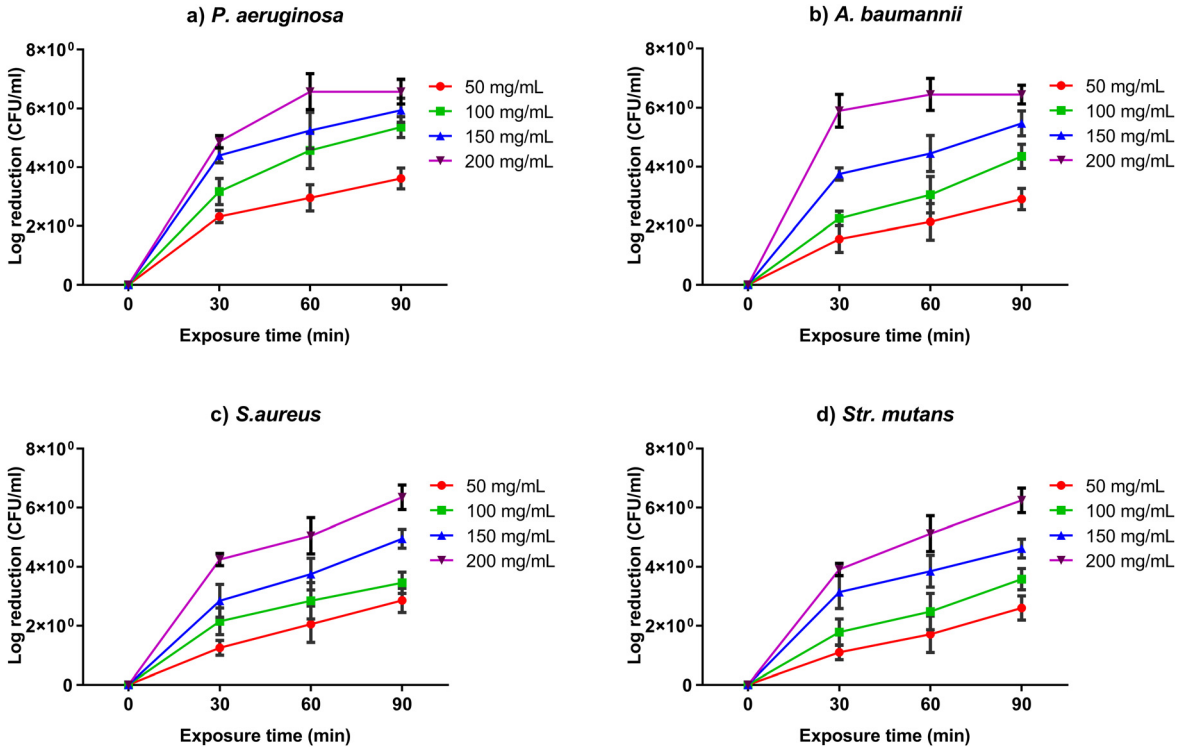

Fig. 2 Log reduction count of selected bacterial strains namely (a) *P. aeruginosa*, (b) *A. baumannii*, (c) *S. aureus*, and (d) *Str. mutans* after exposure to Cinnam at different dosages (50–200 μg mL^{-1}) within the various times of exposure (0–90 min).

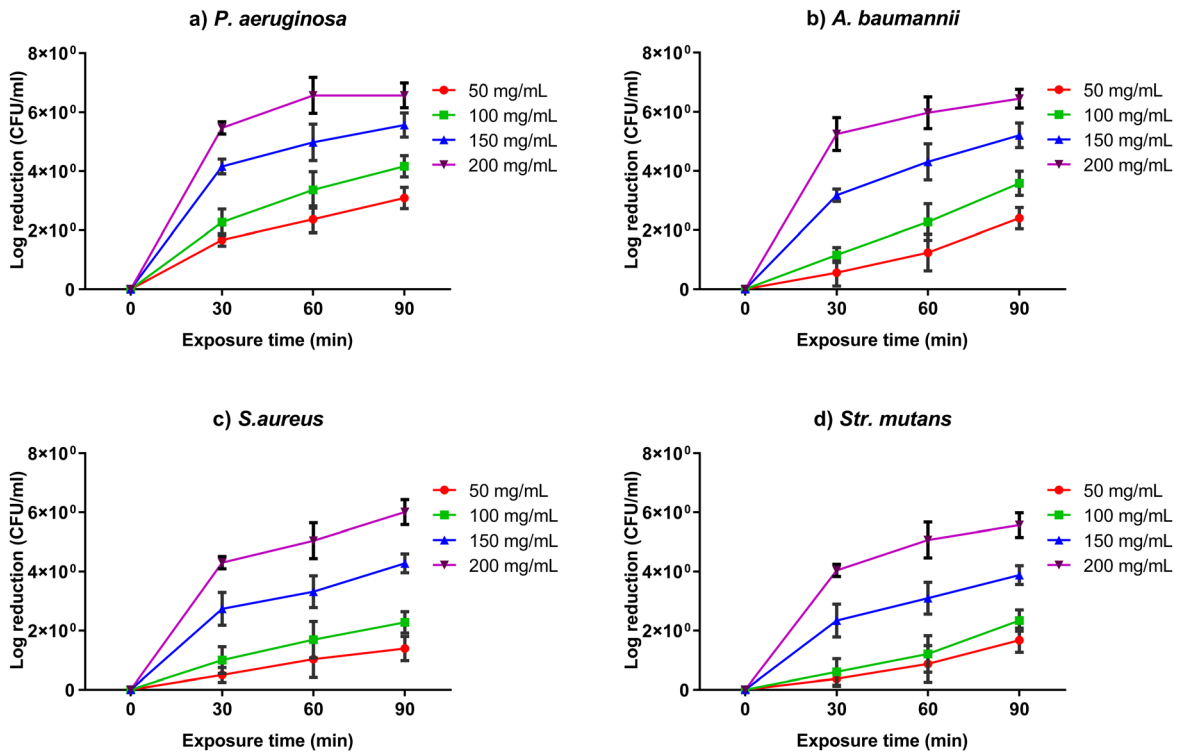

Fig. 3 Log reduction count of selected bacterial strains namely (a) *P. aeruginosa*, (b) *A. baumannii*, (c) *S. aureus*, and (d) *Str. mutans* after exposure to Anis at different dosages (50–200 μg mL^{-1}) within the various times of exposure (0–90 min).

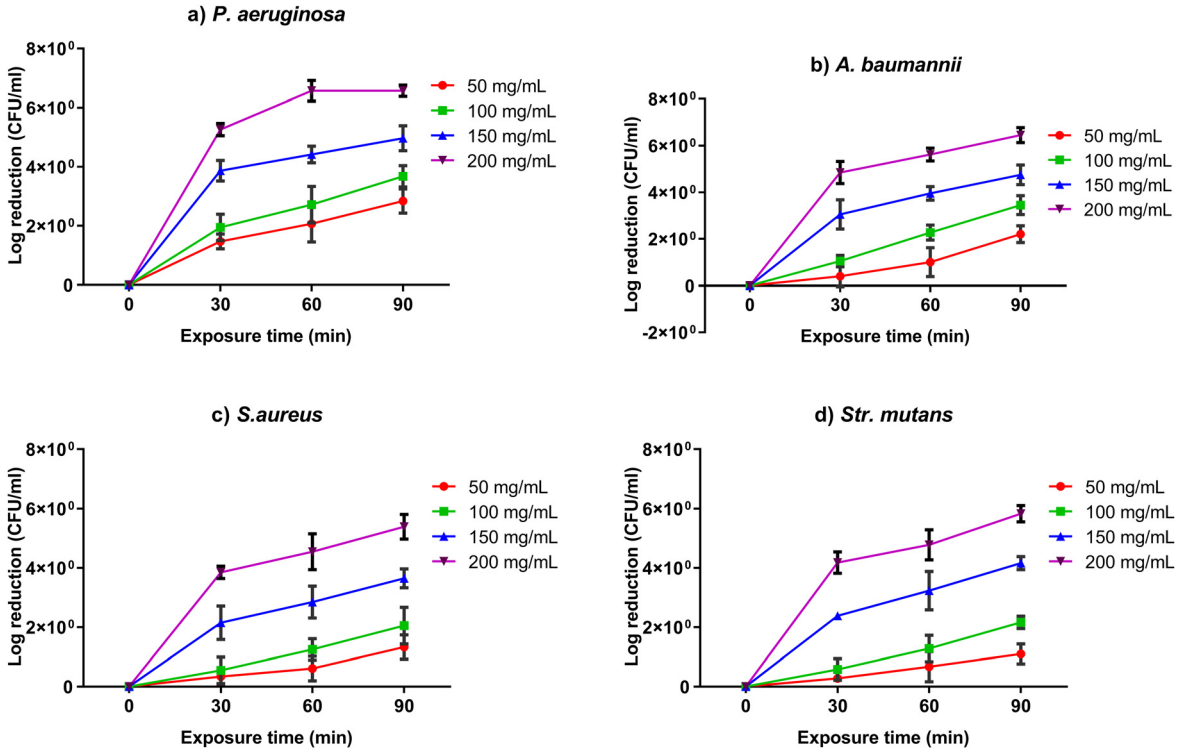

Fig. 4 Log reduction count of selected bacterial strains namely (a) *P. aeruginosa*, (b) *A. baumannii*, (c) *S. aureus*, and (d) *Str. mutans* after exposure to Phenylact at different dosages (50–200 μg mL^{-1}) within the various times of exposure (0–90 min).

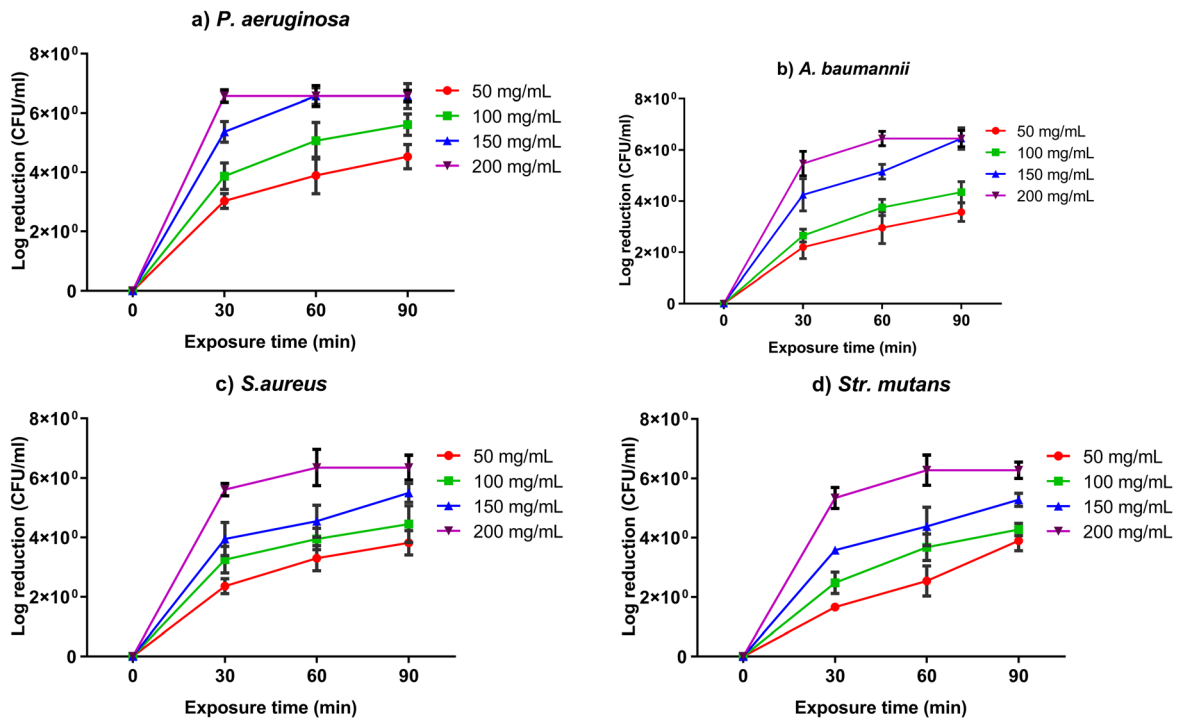

Fig. 5 Log reduction count of selected bacterial strains namely (a) *P. aeruginosa*; (b) *A. baumannii*; (c) *S. aureus*, (d) *Str. mutans* after exposure to Syring at different dosages (50–200 μg mL^{-1}) within the various times of exposure (0–90 min).

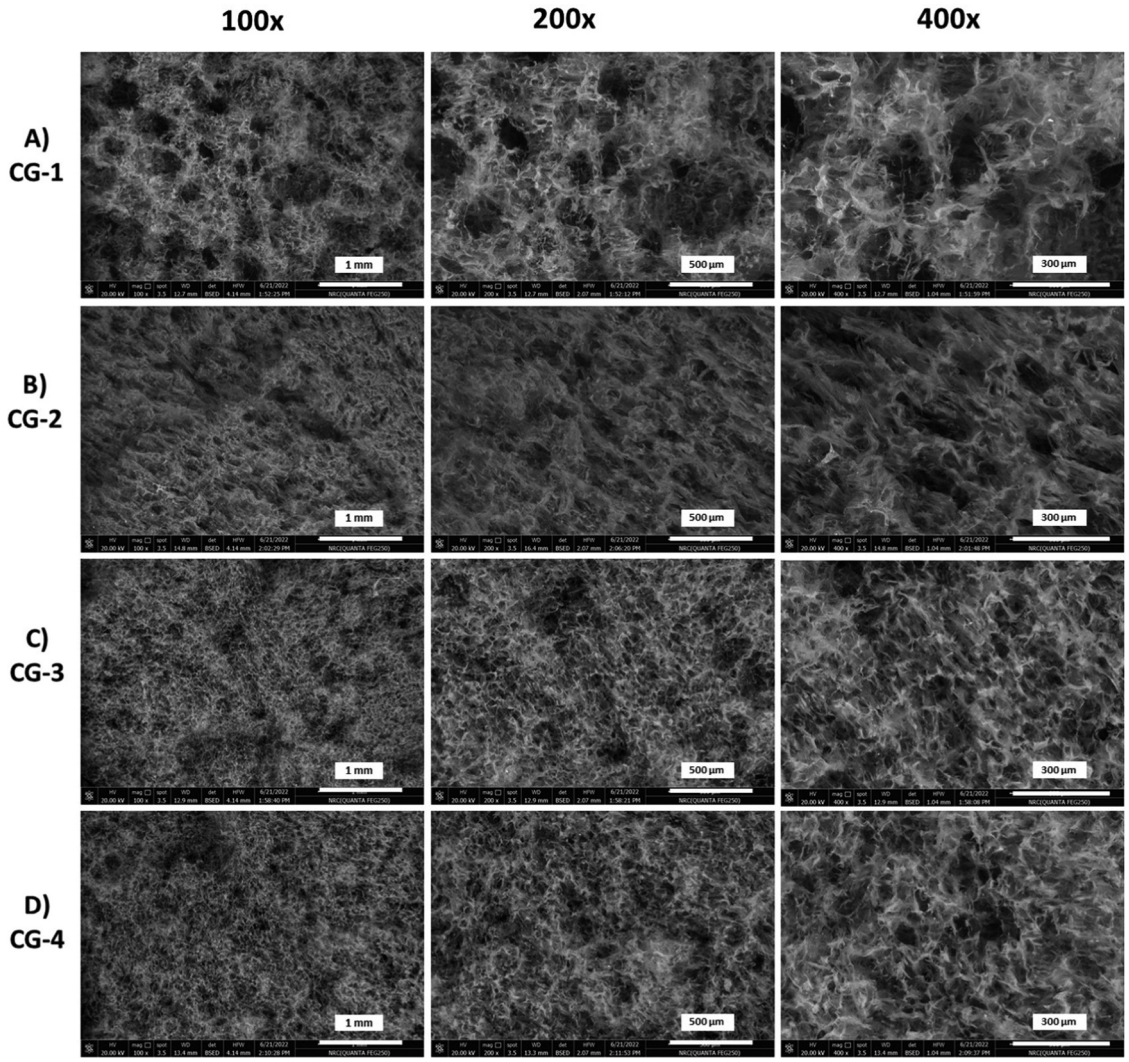

Fig. 6 Scanning electron microscopy images of PVA-P/PVA-F cryogels: (A) CG-1 (95/5); (B) CG-2 (90/10); (C) CG-3 (80/20); and (D) CG-4 (50/50) augmented with CNFs and taken at different magnifications namely 100, 200, and 400×.

occurring chemical that can be obtained. It is mainly composed of natural sources of compounds derived from plants such as *Phragmites vallatoria* and others in the Poaceae family. Antioxidant, bactericidal, and other medicinal properties are all represented in this molecule. The compound was capable of minimizing the antibiotic dosage required to inhibit the growth of drug-resistant bacteria (tetracycline, norfloxacin, and ethidium bromide), demonstrating the capacity of syringaldehyde to inhibit the efflux pump on these bacteria.[48,49]

3.3. Characterization of the cryogel

Porous structures like xerogels, cryogels and aerogels are recognized as highly porous drug delivery vehicles where their porosity percentage depends on the fabrication technique.[50] Aerogels exhibit the highest porosity among all and can be fabricated *via* supercritical carbon dioxide drying, where solvents are exchanged by CO_2 gas. On the other hand, xerogels are produced by air-drying wet gels producing a low pore volume material. Nevertheless, cryogels possess an intermediate pore density produced *via* the freeze-drying technique. The presence of such pores in the structures of these materials enhances their swelling in physiological fluids and offers an ideal space for loading drugs.[51] In the current research, cryogel systems were produced through three stages; solution mixing, followed by gelation and finally drying. At first, the solution stage involved the blending of two polyvinyl alcohol grades, partially (PVA-P) and fully (PVA-F) hydrolyzed, in different ratios with cellulose nanofibrils (CNFs). In the second stage, the gelling occurred through the formation of inter and intramolecular hydrogen bonding between the PVA and CNF hydroxyl groups followed by the development of nano and micropores with the aid of PVA-F.[52] The second stage also involved the freezing of the gel at −5 °C to keep the ice crystal zone without disturbance. We used PVA-F as a network-making material because its chains were proven to cross-link upon freezing and thawing cycles.[53] PVA chains can develop an organized structure called a microcrystalline zone that serves as the network's junction knots. At these knots, PVA macro-chains establish abundant hydrogen bonds. Another interpretation for

junction zone formation is the forced alignment of PVA-F polymeric chains when concentration enhanced by the transformation of water into ice may offer a mechanism for the establishment of side by side associations that are preserved upon thawing or drying. In such a case, the system does not need an additional cross-linker to maintain the integrity of its structure upon coming into contact with water or body fluids. The third stage involved drying at −60 °C under vacuum to allow sublimation of the entrapped solvent from the cryogel pores without causing any morphological deuteriation.[54]

3.3.1. Surface morphology. Fig. 6 shows the cross-section morphology of the cryogel samples (CG-1, CG-2, CG-3, and CG-4) at different magnifications, namely 100, 200, and 400×. The porosity of the cryogels formed as a result of the evaporation of ice crystals after being placed in a high vacuum chamber.[55] All samples exhibited micropore structures and no lamellar structure could be seen. This could be explained by the fact that PVA-F tends to cross-link and form gels slowly after it dissolves; therefore, tiny pores were formed rather than interconnected lamellar structures. Moreover, the pore size of the cryogels decreased as the ratio of the PVA-F increased in the blend from 5%, in CG-1, to 50%, in CG-4. As the PVA-F ratio increases in the system, the cross-linking tendency increased possibly due to the formation of more junction zones.[56] Other literature reports interpreted the shrinking pore of the PVA-F cryogel as a result of vacuum drying and the percentage of an additional polymer, PVA-P in this case. Increasing the PVA-P content decreased the shrinking of freeze-dried cryogels because PVA-P, as a second polymer in the structure of samples, did not crosslink; this was reflected in the pore uniformity distribution of the cryogel samples.[57] On the other hand, the presence of CNFs in the system helped the formation of an interconnected network in the PVA molecular chains and delayed the gel formation leading to the formation of stable pores. The porous structure of cryogels plays a crucial role in drug loading and release kinetics.

3.3.2. Surface area, swelling, mechanical compression, and drug release. The dry cryogels showed minimal shrinkage and were gently removed from the plastic molds for further investigation. The surface area and swelling characteristics were assessed to determine their potential for drug loading. It is clear from Fig. 7(A) that all samples were intact disks without any damage; however, CG-1, CG-2, and CG-3 partially disintegrated and deformed during the swelling experiment, after being submerged in saline solution for 24 h. On the other hand, CG-4 remained undeformed. This behavior could be explained by the increment of the PVA-F ratio in the samples (5% in CG-1 *versus* 50% in CG-4), which led to a higher cross-linking degree between the other component, PVA-P, and CNFs. These observations are consistent with the swelling percentages presented in Fig. 7(B), where CG-1 was able to hold water with around two-fold its dry weight. The swelling percentage increased as the percentage of PVA-F ratio increased in the sample and reached 1600% for CG-4. The entanglement of polymer chains as a result of crosslinking is reflected in physical properties such as the

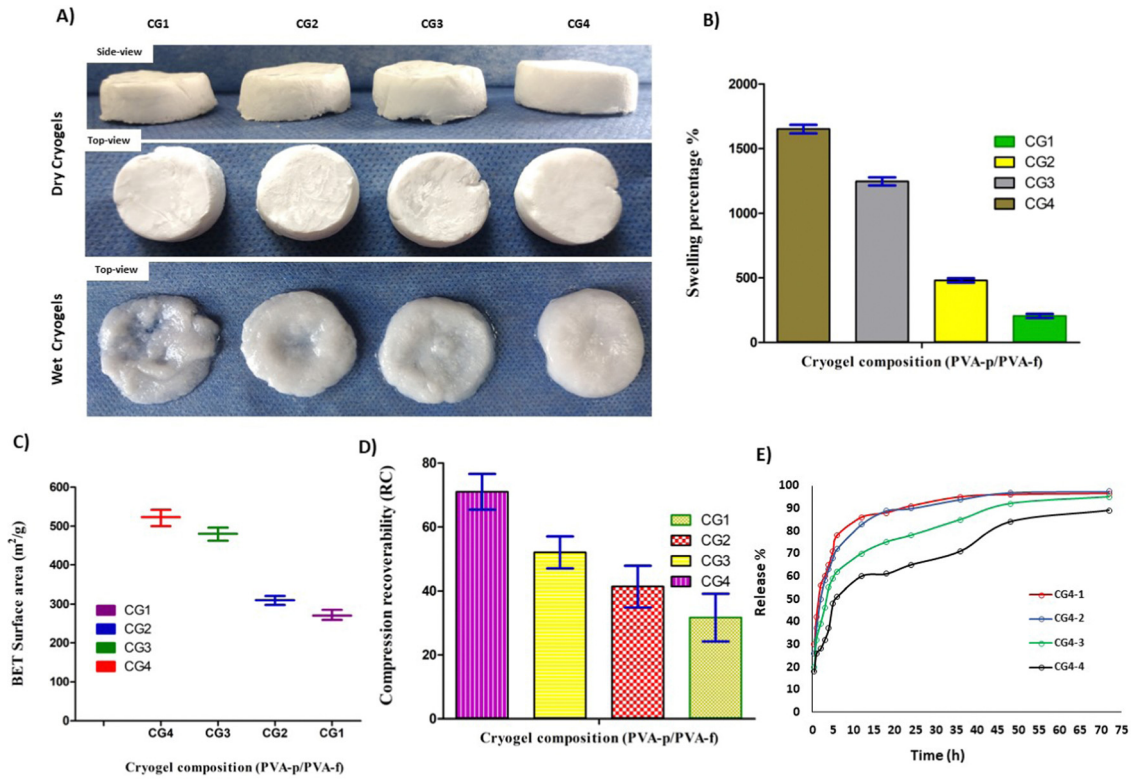

Fig. 7 Physiochemical properties of CG-1, CG-2, CG-3, and CG-4 cryogels. (A) photo images of dry and wet cryogels, (B) swelling percentage, (C) surface area, (D) mechanical compression, and (E) release profile of the Cinnam derivative.

swelling ratio. If the degree of crosslinking is low, the physical interaction between polymers breaks easily, forming hydrogels with slight swelling properties. However, as the crosslinking degree increases, more crosslinking points form, leading to more swelling.[58] Furthermore, an increment of crosslinking makes the cryogels have more elastic pores, leading to more swelling properties. Crosslinking can make polymers elastic, allowing more water holding which will be reflected in the swelling ratio. It is worth noticing that increasing the crosslinking after a certain threshold will cause the stiffening of the pores which will be correlated with a decrement in the swelling ratio.[59]

The surface area values and the mechanical compression data of the cryogels also showed the same increment trend as presented for their swelling ratio. Fig. 7(C) depicts the surface area expressed by the square meter per gram of the samples. CG-1 and CG-2 showed close values, 270 and 310 $m^2\ g^{-1}$, respectively. However, CG-3 and CG-4 showed surface areas of 480 and 523 $m^2\ g^{-1}$, respectively. BET areas are typically quite sensitive to the pore size, structural heterogeneity, and interactions between the adsorbate and the adsorbent. It is well recognized that the BET method's relevance to the assessment of porosity is difficult since it is unable to capture complicated adsorption mechanisms because of the impacts of micropore filing.[60] BET results showed an increasing trend with an increase in the PVA-F percentage. It is established that large pore-size scaffolds prepared by freeze-drying (lyophilization) provide better nutrient supply and the surface area and mechanical properties in terms of recoverability decrease as a result of the increased pore size.[61] Another literature indicated that a clear relationship is evident between the pore size and the resulting surface area of scaffolds; the data indicated that by increasing the pore size, the specific surface area or the amount of material present in an average pore increases.[62,63] For the same reason, the mechanical behavior of CG-4, represented by compression recoverability (Fig. 7(D)), was the highest among all samples, 72%.

Based on the above-discussed results, sample CG4 was recognized as the best-performing drug carrier candidate. Four different concentrations of the Cinnam aminophosphonate drug (0.25, 0.5, 1, and 2 mg in 5 mL of polymer blend) were prepared and loaded into CG-4 cryogel samples and the release behavior was studied. Fig. 7(E) shows the release of the Cinnam aminophosphonate drug. Cryogel CG-1 with the lowest concentration showed burst release at first 5 h as a result of rapid dissolution and diffusion rate. On the other hand, as the drug concentration increased, the release showed more sustainable behavior due to lower dissolution and diffusion processes. The higher drug concentration in CG-4 showed higher sustained drug release based on the cumulative release data. The low cumulative release is due to drug precipitation which could be due to either high drug concentrations or drug water insolubility as in the case of the Cinnam aminophosphonate drug.[64]

3.4. Determination of the antimicrobial efficacy and biofilm development of drug-loaded cryogels

3.4.1. Qualitative and quantitative antimicrobial efficacy evaluation of cryogels. The Cinnam drug was successfully incorporated in CG-4 with different ratios and constant concentrations of Cinnam. The antibacterial efficacy of four prepared cryogels, including CG4-1, CG4-2, CG4-3, and CG4-4 was assessed using the disk diffusion assay. The sample CG4-4 exhibited the highest antibacterial activity against *A. baumannii*, *P. aeruginosa*, *S. aureus*, and *Str. mutans* with ZOIs of 31.4 ± 0.46, 27.4 ± 0.20, 24.2 ± 0.38, and 22 ± 0.53 mm, respectively. However, the lowest antibacterial effect against selected bacterial pathogens was recorded to be CG4-1, where the widths of the ZOI for *A. baumannii*, *P. aeruginosa*, *S. aureus*, and *Str. mutans* were 10.5 ± 0.34, 8.6 ± 0.26, 7.2 ± 0.27, and 6.3 ± 0.34 mm, respectively (Table 2 and Fig. 8). Regarding the unloaded cryogel, the results revealed that there was no antibacterial effect against the tested bacteria.

Table 2 Diameters of the ZOI (mean ± SD) in mm of the four loaded cryogels against different types of skin pathogenic bacteria using the disk diffusion assay

	ZOI diameter in mm			
Sample	*P. aeruginosa*	*A. baumannii*	*S. aureus*	*Str. mutans*
CG4-1	10.5 ± 0.34^{c}	8.6 ± 0.26^{b}	7.2 ± 0.27^{b}	6.3 ± 0.34^{b}
CG4-2	18.7 ± 0.17^{d}	16.4 ± 0.27^{c}	14 ± 0.11^{b}	12.4 ± 0.76^{b}
CG4-3	23 ± 0.42^{d}	21.5 ± 0.52^{c}	19.8 ± 0.38^{c}	17.6 ± 0.64^{c}
CG4-4	31.4 ± 0.46^{d}	27.4 ± 0.20^{d}	24.2 ± 0.38^{c}	22 ± 0.53^{c}
dH_2O	0.00^{a}	0.00^{a}	0.00^{a}	0.00^{a}
Cip.	15.3 ± 0.36^{c}	13 ± 0.48^{d}	11.8 ± 0.23^{c}	10 ± 0.12^{d}

00 = no zone. Each value is the average of three replicates (mean ± SD). Different lowercase letters (a–d) refer to mean values with significantly different values ($p < 0.05$) between the tested samples in each particular bacterium/fungus.

Fig. 9 presents the time-dependent bacterial survival count after individual treatment with four drug-loaded cryogels to establish the effectiveness of bacterial killing against various skin pathogenic bacterial species. The most vigorous bactericidal activity was found for CG-4-4 against all relevant bacterial strains tested as denoted by the solid red line. Initially, t CG-4-4 could efficiently eradicate both Gram-negative and Gram-

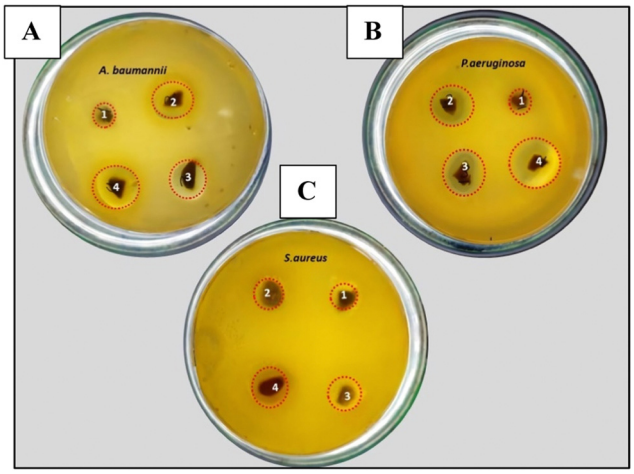

Fig. 8 Image of *in vitro* antibacterial properties using the disk diffusion assay of four cryogels (1: CG4-1, 2: CG4-2, 3: CG4-3, and 4: CG4-4) against (A) *A. baumannii*; (B) *P. aeruginosa*; and (C) *S. aureus*.

positive bacteria. The results showed a more than 6 log CFU reduction within 3 h for *P.aeruginosa*, 4 h for *A.baumannii*, and 5 h for *S.aureus* and *Str.mutans*. Even though CG-4-3, as illustrated by the blue line, had an equivalent destructive impact on bacterial pathogens, the exposure duration was longer than CG-4. The results revealed that CG-4-4 could effectively remove bacterial cells after only a few minutes of exposure. In addition, when compared to Gram +ve species like *S. aureus* and *Str.mutans*, the CG-4-4 showed rapid and effective antibacterial activity against Gram -ve species, including *A. baumannii* and *P. aeruginosa*. Interestingly, CG-4-1 displayed the most minor antibacterial activities against all selected pathogenic bacteria, despite the fact that even the highest dose and longest exposure duration could not completely eliminate the bacteria.

3.4.2. Effects of the drug-loaded cryogels on biofilm development. To investigate the impact of cryogels on selected species of bacteria in a biofilm form, each strain's monospecies bacterial biofilm was investigated over various incubation days (3, 5, 7, and 14 days) as illustrated in Fig. 10. The results indicated that the rate of biofilm development was significantly altered for CG-4-4, which prohibited bacterial colonization. After 3–14 days of incubation in the presence of the obtained bioactive CG4-4, the efficacious inhibitory effects of the tested CG-4-4 against all tested bacterial biofilms were revealed, where the 6 log CFU was reduced of viable biofilm cells developed on the coated glass slides, as compared to uncoated glass slides used as controls. This means that the bacterial cells were unable to stick to the surface owing to the combination of a high concentration of Cinnam (50:50), which permitted the bioactive components to be delivered quickly and continuously for a longer period, defeating biofilm development. On the other hand, the bacterial strains were capable of creating a biofilm in the early stage of biofilm formation, but biofilm production was dramatically reduced within 14 days in the maturation stage.

Interestingly, CG4-1 required a very long time to discharge the active molecules after 14 days of incubation. The present study's results are in line with Wang *et al.*[65] where the effect of Cinnam on the biofilm formation was shown. The compound prevented bacterial colonization at even sub-inhibitory concentration. After assessing the molecule's impact on the biofilm, the morphological changes, cellular membrane disruption, and breakdown of nuclear materials were analyzed. It was shown that increasing the dose resulted in more damage, the morphological alterations were permanent, and the membrane permeability was weakened and decreased. Furthermore, Firmino *et al.*[66] assessed the bactericidal features of Cinnam on the formation of biofilms since the microbial composition is necessary to determine when infection can occur, as well as protection from it. Hence, Cinnam could prohibit the development of a microbial biofilm and colonization. In the same way, Field *et al.*[67] evaluated the biocidal properties of Cinnam incorporated with EDTA toward pathogenic *E. coli*. They displayed that combining Cinnam with another compound increased its antimicrobial potential compared to using it alone.

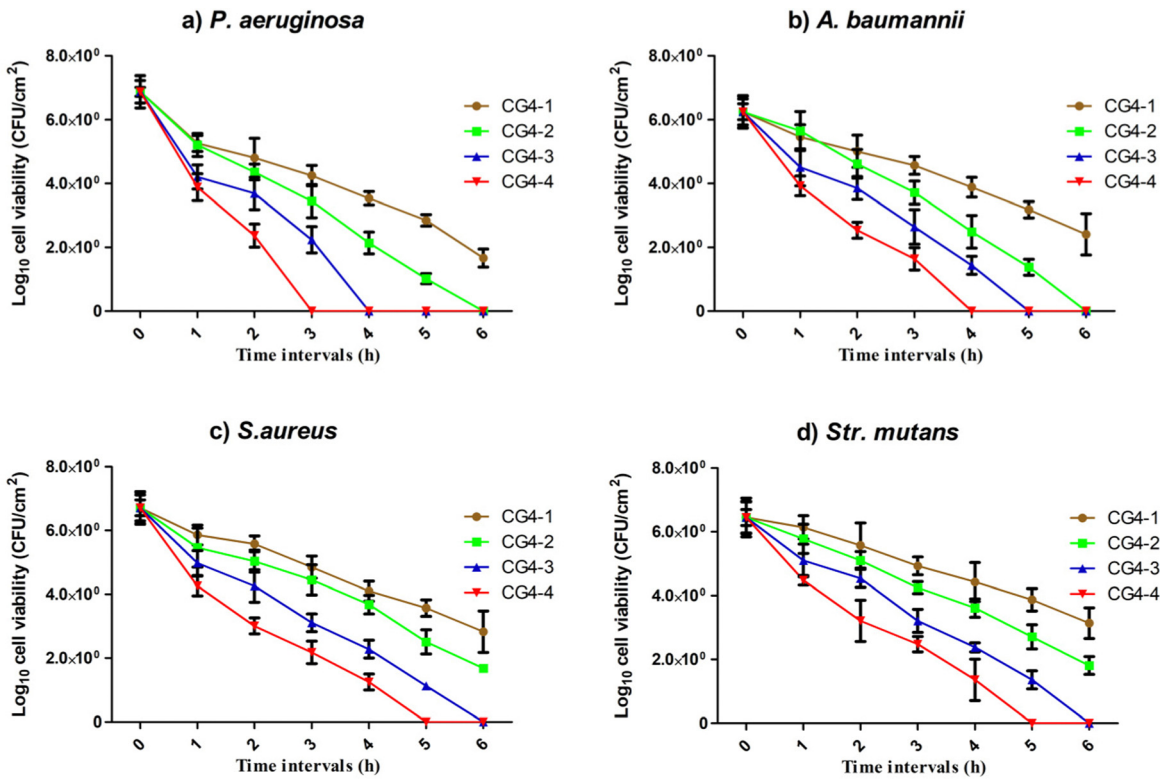

Fig. 9 The time-dependent killing of four cryogels against various skin pathogenic bacteria (a) *P. aeruginosa*; (b) *A. baumannii*; (c) *S. aureus*, and (d) *Str. mutans*. The samples were withdrawn at the determined time of exposure (1–6 h).

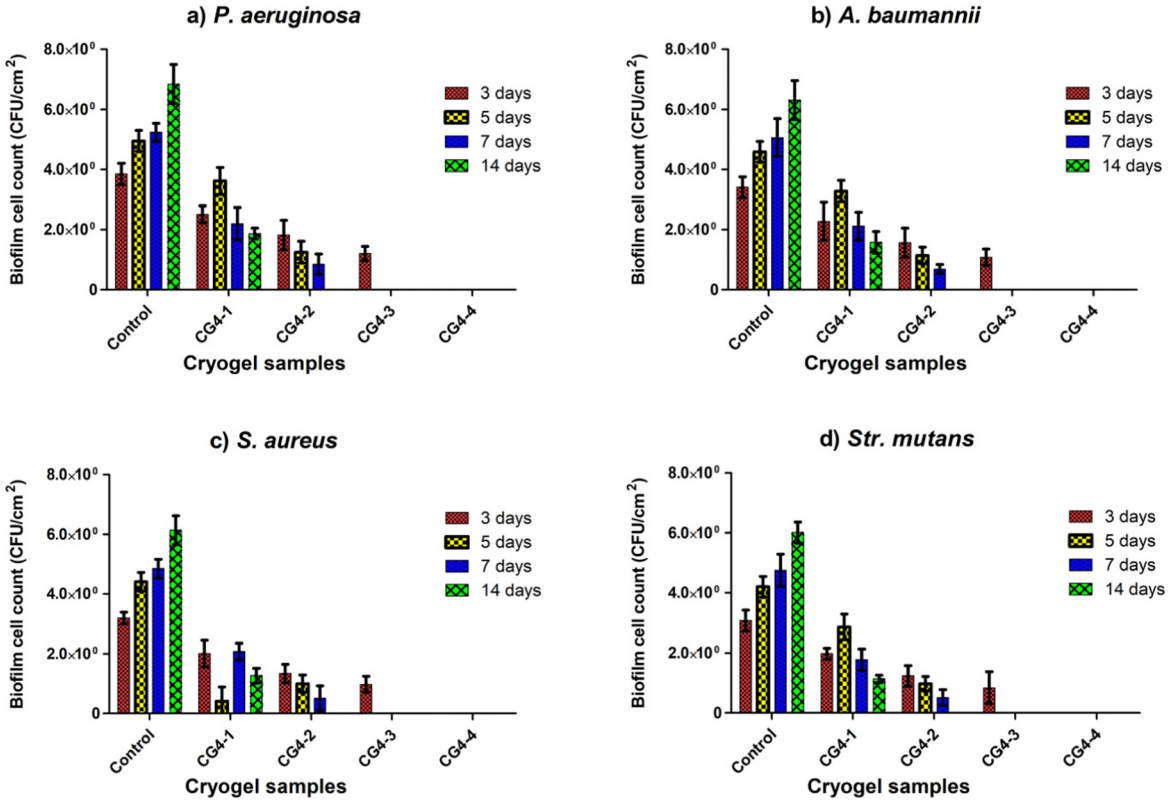

Fig. 10 Logs of the viable cell number of monospecies bacterial biofilms: (a) *P. aeruginosa*, (b) *A. baumannii*, (c) *S. aureus*, and (d) *Str. mutans* developed on studied cryogels.

The toxicological studies proved that all cryogels had no cytotoxic effects and were biocompatible. Therefore, it can be utilized for medical purposes without doubts or fears.

4. Conclusion

The results obtained in this study illustrated the successful production of self-crosslinked tri-component cryogels, using partially hydrolyzed polyvinyl alcohol (PVA-P), fully hydrolyzed polyvinyl alcohol (PVA-F), and cellulose nanofibrils (CNFs), loaded with antimicrobial α-aminophosphonate derivative. Cryogels made from a 50/50 blending ratio of PVA-P/PVA-F and loaded with various concentrations of Cinnam showed antimicrobial and anti-biofilm formation properties against Gram-negative and Gram-positive bacteria and showed sustained drug release profiles by increasing the Cinnam concentration. All these results demonstrated that Cinnam-loaded tri-component cryogels have great potential for use as antimicrobial and anti-biofilm wound dressing materials.

Data availability

The data of this research are available upon request.

Conflicts of interest

There are no conflicts to declare.

References

1 W. K. Stadelmann, A. G. Digenis and G. R. Tobin, *Am. J. Surg.*, 1998, **176**, 26S–38S.
2 J. B. Wright, K. Lam, A. G. Buret, M. E. Olson and R. E. Burrell, *Wound Repair Regen.*, 2002, **10**, 141–151.
3 B. Nutan and A. K. S. Chandel, *Antimicrobial Dressings*, Elsevier, 2023, pp. 187–202.
4 K. K. Ahmed and A. Wongrakpanich, *Ther. Delivery*, 2022, **13**, 489–505.
5 P. R. Varga and G. Keglevich, *Molecules*, 2021, **26**, 2511.
6 P. R. Varga, K. Karaghiosoff, É. V. Sári, A. Simon, L. Hegedűs, L. Drahos and G. Keglevich, *Org. Biomol. Chem.*, 2023, **21**, 1709–1718.
7 D. Kocsis, P. R. Varga, R. Keshwan, M. Nader, M. Lengyel, P. Szabó, I. Antal, K. Kánai, G. Keglevich and F. Erdő, *Pharmaceutics*, 2023, **15**, 1464.
8 D. A. Elsherbiny, A. M. Abdelgawad, T. I. Shaheen, N. A. Abdelwahed, S. Jockenhoevel and S. Ghazanfari, *Int. J. Biol. Macromol.*, 2023, **233**, 123655.
9 C. K. Field and M. D. Kerstein, *Am. J. Surg.*, 1994, **167**, S2–S6.
10 S. A. Jones, P. G. Bowler, M. Walker and D. Parsons, *Wound Repair Regen.*, 2004, **12**, 288–294.
11 Y. Li, L. Su, Y. Zhang, Y. Liu, F. Huang, Y. Ren, Y. An, L. Shi, H. C. van der Mei and H. J. Busscher, *Adv. Sci.*, 2022, **9**, 2103485.
12 Y. Li, J. Chi, P. Xu, X. Dong, A.-T. Le, K. Shi, Y. Liu and J. Xiao, *J. Mater. Sci. Technol.*, 2023, **155**, 238–252.

13 B. Akin and M. M. Ozmen, *Prog. Biomater.*, 2022, **11**, 331–346.
14 G. Xu, N. Xu, T. Ren, C. Chen, J. Li, L. Ding, Y. Chen, G. Chen, Z. Li and Y. Yu, *Int. J. Biol. Macromol.*, 2022, **208**, 760–771.
15 Y. Yang, M. Li, G. Pan, J. Chen and B. Guo, *Adv. Funct. Mater.*, 2023, 2214089.
16 J. H. Jung, J. H. Lee, J. R. Silverman and G. John, *Chem. Soc. Rev.*, 2013, **42**, 924–936.
17 Y. Zhang, J. Zhang, T. Jiang and S. Wang, *Int. J. Pharm.*, 2011, **410**, 118–124.
18 J. B. Wolinsky, Y. L. Colson and M. W. Grinstaff, *J. Controlled Release*, 2012, **159**, 14–26.
19 C. Tan, B. M. Fung, J. K. Newman and C. Vu, *Adv. Mater.*, 2001, **13**, 644–646.
20 M. S. Toivonen, A. Kaskela, O. J. Rojas, E. I. Kauppinen and O. Ikkala, *Adv. Funct. Mater.*, 2015, **25**, 6618–6626.
21 F. Wang, J. Sun, H. Shi, J. Zhou, X. Ma, X. Song, X. Su and L. Liu, *Int. J. Biol. Macromol.*, 2023, **224**, 1373–1381.
22 P. Kueseng, C. Thammakhet, P. Thavarungkul and P. Kanatharana, *Microchem. J.*, 2010, **96**, 317–323.
23 N. Kathuria, A. Tripathi, K. K. Kar and A. Kumar, *Acta Biomater.*, 2009, **5**, 406–418.
24 S. Bhat, A. Tripathi and A. Kumar, *J. R. Soc., Interface*, 2011, **8**, 540–554.
25 A. M. Abdelgawad, M. E. El-Naggar, D. A. Elsherbiny, S. Ali, M. S. Abdel-Aziz and Y. K. Abdel-Monem, *J. Environ. Chem. Eng.*, 2020, **8**, 104276.
26 K. Katopodis, A. Kapourani, E. Vardaka, A. Karagianni, C. Chorianopoulou, K. N. Kontogiannopoulos, D. N. Bikiaris, K. Kachrimanis and P. Barmpalexis, *Int. J. Pharm.*, 2020, **578**, 119121.
27 S. Virtanen, J. Vartianen, H. Setälä, T. Tammelin and S. Vuoti, *RSC Adv.*, 2014, **4**, 11343–11350.
28 M. S. Peresin, Y. Habibi, A.-H. Vesterinen, O. J. Rojas, J. J. Pawlak and J. V. Seppala, *Biomacromolecules*, 2010, **11**, 2471–2477.
29 H. S. Mansur, C. M. Sadahira, A. N. Souza and A. A. Mansur, *Mater. Sci. Eng., C*, 2008, **28**, 539–548.
30 X. Xu, F. Liu, L. Jiang, J. Zhu, D. Haagenson and D. P. Wiesenborn, *ACS Appl. Mater. Interfaces*, 2013, **5**, 2999–3009.
31 R. Nagarkar and J. Patel, *Acta Pharm. Sci.*, 2019, **3**, 34–44.
32 H. Seddiqi, E. Oliaei, H. Honarkar, J. Jin, L. C. Geonzon, R. G. Bacabac and J. Klein-Nulend, *Cellulose*, 2021, **28**, 1893–1931.
33 S. Moritz, C. Wiegand, F. Wesarg, N. Hessler, F. A. Müller, D. Kralisch, U.-C. Hipler and D. Fischer, *Int. J. Pharm.*, 2014, **471**, 45–55.
34 N. Lin and A. Dufresne, *Eur. Polym. J.*, 2014, **59**, 302–325.
35 D. L. S. Scheffel, D. G. Soares, F. G. Basso, C. A. de Souza Costa, D. Pashley and J. Hebling, *J. Dent.*, 2015, **43**, 997–1006.
36 D. A. Elsherbiny, A. M. Abdelgawad, M. E. El-Naggar, R. A. El-Sherbiny, M. H. El-Rafie and I. E.-T. El-Sayed, *Int. J. Biol. Macromol.*, 2020, **163**, 96–107.
37 A. B. Abou Hammad, B. A. Hemdan and A. M. El Nahrawy, *J. Environ. Manage.*, 2020, **270**, 110816.
38 R. Baird, A. Eaton and E. Rice, *Standard Methods for the Examination of Water and Wastewater*, American Public Health Association, American Water Works Association, Water Environment Federation, Washington D.C., 23rd edn, 2017.
39 K. Krishna Rao, M. Subha, B. Vijaya Kumar Naidu, M. Sairam, N. Mallikarjuna and T. Aminabhavi, *J. Appl. Polym. Sci.*, 2006, **102**, 5708–5718.
40 A. M. El Nahrawy, A. Elzwawy, M. Alam, B. A. Hemdan, A. M. Asiri, M. R. Karim, A. B. Abou Hammad and M. M. Rahman, *Microchem. J.*, 2021, **163**, 105881.
41 M. E. El-Naggar, A. M. Abdelgawad, R. Abdel-Sattar, A. A. Gibriel and B. A. Hemdan, *Eur. Polym. J.*, 2023, **184**, 111782.
42 T.-F. He, L.-H. Wang, D.-B. Niu, Q.-H. Wen and X.-A. Zeng, *Arch. Microbiol.*, 2019, **201**, 451–458.
43 Y. Ding, X. Hu, Y. Piao, R. Huang, L. Xie, X. Yan, H. Sun, Y. Li, L. Shi and Y. Liu, *ACS Nano*, 2023, **17**, 6601–6614.
44 N. M. Boshta, E. A. Elgamal and I. E. El-Sayed, *Monatsh. Chem.*, 2018, **149**, 2349–2358.
45 J. F. Malheiro, J.-Y. Maillard, F. Borges and M. Simões, *Int. Biodeterior. Biodegrad.*, 2019, **141**, 71–78.
46 W. Yuan and H.-G. Yuk, *Appl. Environ. Microbiol.*, 2019, **85**, e00271.
47 W. A. Pereira, C. D. S. Pereira, R. G. Assunção, I. S. C. da Silva, F. S. Rego, L. S. Alves, J. S. Santos, F. J. R. Nogueira, A. Zagmignan and T. T. Thomsen, *Biomolecules*, 2021, **11**, 302.
48 S. G. d Brito-Filho, J. K. d S. Maciel, Y. C. F. Teles, M. M. M. d S. Fernandes, O. S. Chaves, M. D. L. Ferreira, P. D. Fernandes, L. P. Felix, I. C. d S. Cirino and J. P. Siqueira-Júnior, *Rev. Bras. Farmacogn.*, 2017, **27**, 453–458.
49 E. Hochma, L. Yarmolinsky, B. Khalfin, M. Nisnevitch, S. Ben-Shabat and F. Nakonechny, *Processes*, 2021, **9**, 2089.
50 A. Muhammad, D. Lee, Y. Shin and J. Park, *Polymers*, 2021, **13**, 1347.
51 L. Zheng, S. Zhang, Z. Ying, J. Liu, Y. Zhou and F. Chen, *Int. J. Nanomed.*, 2020, 2363–2378.
52 A. Azmi, K. S. Lau, S. X. Chin, P. S. Khiew, S. Zakaria and C. H. Chia, *Cellulose*, 2021, **28**, 2241–2253.
53 H. Zhang, F. Zhang and J. Wu, *React. Funct. Polym.*, 2013, **73**, 923–928.
54 D. Lee, J. Kim, S. Kim, G. Kim, J. Roh, S. Lee and H. Han, *Microporous Mesoporous Mater.*, 2019, **288**, 109546.
55 N. Bahrami, M. Bayat, A. Farzin, M. S. Hajseyedjavadi, A. Goodarzi, M. Salehi, R. Karimi, A. Mohamadnia, A. Ahmadi and M. Khanmohammadi, *Arch. Neurosci.*, 2019, **6**, e85118.
56 H. Adelnia, R. Ensandoost, S. S. Moonshi, J. N. Gavgani, E. I. Vasafi and H. T. Ta, *Eur. Polym. J.*, 2022, **164**, 110974.
57 M. Bahadoran, A. Shamloo and Y. D. Nokoorani, *Sci. Rep.*, 2020, **10**, 1–18.
58 N. Varshney, A. K. Sahi, S. Poddar, N. K. Vishwakarma, G. Kavimandan, A. Prakash and S. K. Mahto, *ACS Appl. Mater. Interfaces*, 2022, **14**, 14033–14048.
59 S. Hua, H. Ma, X. Li, H. Yang and A. Wang, *Int. J. Biol. Macromol.*, 2010, **46**, 517–523.
60 J. W. Yun Tian, *AIChE J.*, 2018, **64**, 286–293.
61 A. Samourides, L. Browning, V. Hearnden and B. Chen, *Mater. Sci. Eng., C*, 2020, **108**, 110384.

62 F. J. O'Brien, B. A. Harley, M. A. Waller, I. V. Yannas, L. J. Gibson and P. J. Prendergast, *Technol. Health Care*, 2007, **15**, 3–17.
63 J. Krieghoff, A.-K. Picke, J. Salbach-Hirsch, S. Rother, C. Heinemann, R. Bernhardt, C. Kascholke, S. Möller, M. Rauner and M. Schnabelrauch, *Biomater. Res.*, 2019, **23**, 1–13.
64 A. Abdel-Mohsen, A. Aly, R. Hrdina, A. Montaser and A. Hebeish, *J. Polym. Environ.*, 2011, **19**, 1005–1012.
65 Y. Wang, Y. Zhang, Y.-Q. Shi, X.-H. Pan, Y.-H. Lu and P. Cao, *Microb. Pathog.*, 2018, **116**, 26–32.
66 D. F. Firmino, T. T. Cavalcante, G. A. Gomes, N. Firmino, L. D. Rosa, M. G. de Carvalho and F. E. Catunda Jr, *Sci. World J.*, 2018, 7405736.
67 D. Field, I. Baghou, M. C. Rea, G. E. Gardiner, R. P. Ross and C. Hill, *Antibiotics*, 2017, **6**, 35.